2013

Fluidization of Fine Powders: Cohesive versus Dynamic Aggregation

Jose Manuel Valverde
University of Seville, Spain

FLUIDIZATION OF FINE POWDERS: COHESIVE VERSUS DYNAMIC AGGREGATION

Jose Manuel Valverde
Faculty of Physics, University of Seville
Avda. Reina Mercedes s/n, 41012 Seville, Spain
T: +34-954550960; F: +34-954239434; E: jmillan@us.es

ABSTRACT

Most empirical observations and numerical analyses have demonstrated that gas-fluidized beds of granular materials can only be stabilized if interparticle attractive forces reach an order of magnitude similar to particle weight. If attractive forces are only determined by the universal van der Waals interaction, this occurs when particle size is typically of the order of a few tens of microns. In the absence of sufficiently strong attractive forces, gas-fluidized beds exhibit an unstable bubbling behavior. On the other side, powders with particle size smaller than about 20 microns cannot be fluidized by a gas because interparticle forces are exceedingly large as compared to particle weight, which leads to cohesive aggregation. Cohesive aggregates reaching a large size cannot be disrupted by the gas. The gas flow becomes heterogeneously distributed in the bed and usually bypasses it through channels that hinder the gas-solids contact efficiency. In the last years, a number of reports have appeared on the behavior of a new class of fine and ultrafine powders, which resembles the nonbubbling fluidlike behavior of noncohesive granular materials fluidized by liquids. As opposed to cohesive aggregation, fine particles in these special class of powders undergo a dynamical process of aggregation in the fluidized bed, which gives rise to the formation of light aggregates that can be uniformly fluidized in a fluidlike regime. In this paper, we rationalize this new type of fluidization behavior by considering dynamic aggregates, grown to a size limited by the balance between interparticle force and flow shear, as effective low-density particles.

INTRODUCTION

The classical Geldart's diagram summarizes empirical observations on beds fluidized by dry air at ambient conditions in terms of particle size versus the relative density difference between the solid particles and the gas. A useful nondimensional number to interpret the Geldart's diagram is the granular Bond number Bo_g, defined as the ratio of interparticle attractive force F_0 to particle weight W_p (Valverde 2013). Gas-fluidized beds of granular materials with particle size $d_p \gtrsim 100$ μm ($Bo_g \lesssim 1$) generally bubble just beyond the onset of fluidization (Geldart B behavior) (Geldart

1973). For slightly cohesive powders ($Bo_g \sim 1$), gas-fluidized beds exhibit a uniform fluidization interval at gas velocities above the minimum fluidization velocity. This state is characterized by a stable expansion of the bed prior to the bubbling onset (Geldart A behavior) (Geldart 1973). In the stable fluidization state, the bed behaves like a weak solid due to enduring interparticle contacts caused by interparticle attractive forces, which sustain part of the bed weight (Rietema 1991). Fine powders, with particle size typically $d_p \lesssim 20$ μm ($Bo_g >> 1$), are generally impossible to fluidize uniformly by a gas due to the strong attractive forces existing between the particles when compared to their weight. When fluidized by a gas, fine cohesive powders tend to rise as a slug of solids or to form channels through which the fluid will escape rather than being distributed through the bulk. This heterogeneous fluidization behavior is the so-called Geldart C (cohesive) behavior (Geldart 1973).

Out of the scope of Geldart's classification, there are some fine and ultrafine powders that may reach a highly expanded state of nonbubbling fluidlike fluidization when fluidized by air at ambient conditions (Valverde 2013). Fine powders showing this behavior are conditioned xerographic toners, made of polymer particles with a volume average size $d_p <\sim 10\mu$m. For such a small particle size, we would predict the Geldart C fluidization behavior. However, the addition of fumed silica nanoparticles, which become dispersed on the surface of the toner particles, decreases interparticle adhesion, allowing fluidlike nonbubbling behavior. This type of behavior has been also reported for some nanostructured powders (Zhu et al. 2005) and even in some cases there is a full suppression of the bubbling regime, i.e. the fluidized bed transits directly from a nonbubbling fluidlike behavior to elutriation. Reports of nonbubbling fluidlike fluidization of micron and sub-micron primary particles can be found from the mid-1980s (Chaouki et al. 1985; Brooks and Fitzgerald 1986; Morooka et al. 1988; Pacek and Nienow 1990). A common observation was that uniform fluidization was closely related to the formation of light agglomerates when fluidizing the original powder at a superficial gas velocity much larger than the expected minimum fluidization velocity for the system of individual primary particles. Chaouki et. al. (Chaouki et al. 1985) made a distinction between Geldart C powders and a separate smaller class, C', described as "a typical clustering powder", that fluidized via self-agglomeration of the primary particles, thus behaving as a system of low density fluidizable particles. Since the condition of nonbubbling fluidlike fluidization was intimately related to the formation of porous light agglomerates, this type of fluidization was termed as Agglomerate Particulate Fluidization (APF). More recently, gas-fluidized beds of xerographic toners have been observed to take on many of the properties of a fluid, its upper surface remaining horizontal when the container is tilted and absence of yield stress (Valverde et al. 2001). The extent of the fluidlike regime, and thus the relative role of hydrodynamics on restraining macroscopic bubbling, shortened as particle size was increased (Valverde et al. 2003a). In the limit $Bo_g <\sim 10$, the fluidlike regime shrank to zero and the fluidized bed transited directly from the solid-like to the bubbling regime, indicating that large bubbles could be only restrained by yield stresses for slightly cohesive particles ($Bo_g \sim 1$) as corresponds to the classical Geldart's A type of behavior.

A main feature of the behavior of nonbubbling fluidlike beds of fine powders is that

particles aggregate in the gas phase due to the prevalence of the interparticle attractive force on particle weight by means of a dynamic process ruled by the balance between interparticle attraction and flow gas shear forces on the aggregates (Valverde 2013). However, in order to allow for this dynamic aggregation process between individual fine particles to take place, cohesive aggregates, responsible for the Geldart C behavior must be disrupted by the gas flow down to the scale of particle size. An efficient method to assist fluidization of fine cohesive powders is the addition of surface additives such as silica nanoparticles, which serves to decrease the interparticle adhesive force thus reducing the strength of cohesive aggregates. Otherwise, the strong attractive forces usually existing between fine particles in settled powders cause plastic deformation of contacts, leading to a relevant increase in the adhesive force at interparticle contacts (Castellanos 2005). The attractive force between particles within cohesive aggregates for these powders may be much larger than the van der Waals force due to contact plastic deformation and, if the gas flow cannot break cohesive aggregates of size comparable to the system size, gas channels become rather stable and the fluidized bed exhibits a Geldart C cohesive behavior. The increased contact hardness by means of silica additive surface coverage reduces the adhesive force (Quintanilla et al. 2001), thus allowing for the breaking of interparticle contacts by gas-fluidization. For conditioned powders, the van der Waals force is a good approximation to the interparticle attractive force in fluidization, and individual particles will experience a dynamic process of aggregation. Fluidization assistance techniques to break cohesive aggregates have been also developed to assist fluidization, which serves to turn the Geldart C cohesive fluidization behavior into fluidlike fluidization. Among these methods, we find the application of mechanical agitation (Pfeffer et al. 2004; Quintanilla et al. 2008), sound wave pulsation (Zhu et al. 2004), centrifugation (Quevedo et al. 2007), application of variable electric fields (Lepek et al. 2010; Quintanilla et al. 2012b), addition of large magnetic particles that are excited by a variable magnetic field (Yu et al. 2005), and injection of high velocity jets into the bottom of the bed (van Ommen et al. 2010; Quevedo et al. 2010). A phenomenological approach described in this work to analyze the behavior of gas-fluidized beds of conditioned fine powders is to consider dynamic aggregates as effective lightweight spheres, which may exhibit nonbubbling gas-fluidization similarly to coarse beads fluidized by liquids.

DYNAMIC AGGREGATION OF FINE PARTICLES IN A FLUIDIZED BED

Non-Brownian fine particles suspended in a flowing fluid aggregate through a process driven by the dynamic equilibrium between the weight of the aggregate and the hydrodynamic friction from the surrounding gas. The growth of the aggregate is limited by their mechanical strength, which decreases as its size increases. As the aggregate size increases, its increasing weight has to be balanced by the hydrodynamic drag force from the surrounding fluid. But, while gravity is a body force acting uniformly through the aggregate, the drag acts mainly at the surface of the aggregate (even highly porous aggregates are known to screen the hydrodynamic field very effectively (Sutherland and Tan 1970)). Kantor and Witten (Kantor and Witten 1984) and, more recently, Manley et al. (Manley et al. 2004) have studied the size limit of aggregates

in settling suspensions, which, similarly to aggregates in fluidized beds, cannot grow indefinitely due to shear stresses generated by the fluid surrounding the aggregate during sedimentation. Using a simple spring model for the aggregate, it has been shown (Manley et al. 2004) that the typical strain on the aggregate is $\gamma \sim Nm_pg/K_cR_c$, where N is the number of particles in the aggregate, m_p is the particle mass, K_c is the aggregate spring constant and $R_c = kd_p/2$ is the aggregate radius. K_c is given by k_0/k^β, where K_0 is the interparticle force constant, k is the ratio of aggregate size to particle size, and the elasticity exponent is $\beta = 3$ in the 3D case (Kantor and Webman 1984). Thus the local shear force on the aggregate is $F_s \sim K_0\gamma d_p/2 \sim (m_pg)k^{D+2}$, where D is the fractal dimension of the aggregate ($D = \ln N/\ln k$). Manley et al. (Manley et al. 2004) used a critical value, measured independently, for the maximum strain sustainable by an aggregate in a suspension to calculate its maximum size. More generally, it may be estimated that the critical shear force to halt the aggregation process would be order of the interparticle attractive force $F_s^{max} \sim F_0$, which leads to (Valverde 2013)

$$Bo_g \sim Nk^2 = k^{D+2} \tag{1}$$

Equation 1 provides a simple tool to estimate the size of aggregates of fine particles in a gas-fluidized bed from primary physical parameters such as interparticle attractive force, particle weight, size and density, and aggregate fractal dimension. In the DLA model, which was introduced by Witten and Sander (Witten and Sander 1981), aggregates grow as self-similar fractal patterns ramifying due to the irreversible sticking of particles introduced in a random motion to the aggregate. This gives a fractal dimension $D \equiv \ln N/\ln k = 2.5$, where N is the number of particles in the aggregate and k is the ratio of aggregate size to a particle size. Fluidized bed settling experiments (Valverde 2013) performed on conditioned fine powders with varying particle size (from $d_p \sim 7\mu$m to $d_p \sim 20\mu$m) revealed that the fractal dimension of the aggregates in the fluidized bed was close to $D = 2.5$ in accordance with the DLA model of Witten and Sanders.

THE MAXIMUM SIZE OF STABLE BUBBLES

In their study on fluidlike liquid-fluidized beds, Harrison et al. (Harrison et al. 1961) formulated a simple model to account for isolated bubbles stability. These authors hypothesized that a bubble was no longer stable if its rising velocity U_b exceeded the terminal settling velocity of an individual particle v_{p0}. This hypothesis allowed them to estimate the largest stable size D_b of isolated bubbles by means of a simple equation

$$\frac{D_b}{d_p} \simeq \frac{1}{160}\frac{(\rho_p - \rho_f)^2 g d_p^3}{\mu^2} \tag{2}$$

where ρ_p is the particle density, ρ_f is the fluid density and μ is the fluid viscosity. The Harrison et al. equation (Eq. 2), which was originally formulated to study the behavior of liquid-fluidized beds of noncohesive beads, can be modified to account for

the similar behavior exhibited by gas-fluidized beds of dynamic aggregates in order to estimate the ratio of the largest stable size of gas bubbles relative to the aggregate size d^*. The modified equation that results from the balance of the rising velocity of a gas bubble to the terminal settling velocity of an aggregate $v^* = v_{p0}N/k$ is (Valverde 2013)

$$\frac{D_b}{d^*} \simeq \frac{1}{160} \frac{\rho_p^2 \, g \, d_p^3}{\mu^2} \, Bo_g^{(2D-3)/(D+2)} \tag{3}$$

where the equation for the equilibrium size of dynamic aggregates (Eq. 1) has been used. We should expect bubbling fluidization for $D_b/d^* \gtrsim 10$, whereas for $D_b/d^* \lesssim 10$, it is likely that the small gas bubbles developed do not coalesce into large bubbles for a range of gas velocities in which the bed would exhibit nonbubbling fluidization behavior. As the gas velocity is increased and, consequently, the concentration of these small gas bubbles is increased, it should be expected that the coalescence mechanism leads to the onset of macroscopic bubbling at some critical value of the gas velocity. Using, as typical values for fine powders (Valverde 2013), $F_0 = 5$nN, $d_p = 10\mu$m, and $\rho_p = 1000$kg/m^3, Eq. 3 gives $D_b/d^* \simeq 4$ for fluidization with nitrogen at 300K ($\mu = 1.79 \times 10^{-5}$Pa s), thus predicting a transitional behavior (nonbubbling fluidlike to bubbling) in agreement with experimental observations (Valverde 2013). From Eq. 3, it is clear that a change of gas viscosity may result in a qualitative change of fluidization behavior. For example, we would obtain $D_b/d^* \simeq 1.3$ for fluidization with neon at 300K ($\mu = 3.21 \times 10^{-5}$Pa s), which, theoretically, should result in a qualitative improvement of fluidization uniformity and a delay (and possibly suppression) of the onset of bubbling. According to these estimations, when fluidizing with gases of higher viscosities), and/or powders with smaller particle size it can be $D_b/d^* \lesssim 1$), which would indicate that the bubbling regime is suppressed (Valverde 2013).

ON THE QUESTION OF STABILITY

In contrast with the commonly encountered case of gas-fluidized beds stabilized by yield stresses due to enduring particle networks (Sundaresan 2003), the mechanism that restrains bubbling in gas-fluidized beds of conditioned fine powders must have a purely hydrodynamic origin. From fluidized bed mixing experiments (Valverde et al. 2001), the values inferred for the effective diffusion coefficient was seen to increase strongly with gas velocity up to a maximum value coinciding with the onset of bubbling. According to the experimental values inferred for the diffusion coefficient, it was estimated that the particle fluctuation velocity might reach a maximum value which is two orders of magnitude larger than the gas velocity just before the onset of bubbling. Certainly, such huge fluctuation velocities cannot take place in a hydrodynamically stable suspension. Thus, in spite that macroscopic bubbles are not visible in the nonbubling fluidlike regime of conditioned powders, this cannot be a stable state in the strict sense of the word. Accordingly, local measurements of backscattered light from the fluidized bed and direct visualization of the free surface of nonbubbling gas-fluidized beds showed that, in spite of the uniform smooth expansion exhibited in the fluidlike regime, pseudoturbulent mesoscale structures of size on the order of mm with

short-lived local voids were present (Valverde et al. 2001; Valverde et al. 2003b). As the gas flow was increased the number of local voids detected per unit time increased until, at the bubbling transition, local voids coalesced into large amplitude bubbles and a clear segregation of gas and solid phases occurred (Valverde et al. 2003b). Even though mesoscale structures did not grow into fully-developed bubbles in the nonbubbling interval, their presence alone questions the applicability of hydrodynamic linear stability analyses to predict the onset of bubbling. In accordance with these empirical observations, Koch and Sangani (Koch and Sangani 1999) linear stability analysis indicated that the homogeneous state of a fluidlike gas-fluidized bed is always unstable when the particle-phase pressure is only derived from interparticle interactions via instantaneous hard-sphere collisions and from hydrodynamic interactions. On the other hand, a detailed study of nonbubbling liquid-fluidized beds manifests also the existence of short-lived bubble-like voids (Duru and Guazzelli 2002), further indicating that the nonbubbling regime does not necessarily imply hydrodynamic stability.

According to Wallis stability criterion, bubbles in fluidized beds would be an outcome of the formation of concentration shocks or discontinuities in particle concentration when the propagation velocity of a voidage disturbance u_ϕ surpasses the elastic wave velocity u_e of the bed. Even though Foscolo and Gibilaro (Foscolo and Gibilaro 1984) claimed to invoke the Wallis criterion as a condition for planar shock formation, which was assumed to be the mechanism leading to bubbling, the Wallis criterion is simply a particular way of expressing the criterion of linear stability algebraically (as it was made clear by Jackson (Jackson 2000)). The considerations in the above paragraph clearly indicate that the transition from nonbubbling fluidlike to bubbling cannot be analyzed as the departure from a stable state. A large-amplitude phenomenon, such as bubbling, is beyond the range of linear analysis, which leaves the Wallis criterion without a well-founded physical justification. In spite of this, it is undeniable that predictions obtained by Foscolo and Gibilaro were in good agreement with observations on the initiation of visible bubbling in liquid and gas fluidized beds (Foscolo and Gibilaro 1984). Experimental results were also in agreement with the results predicted form the Wallis criterion under systematic variations of relevant parameters on the bubbling point of gas-fluidized beds such as pressure, temperature and addition of fines (Foscolo and Gibilaro 1987). From this point of view, the Wallis criterion can be taken at least as an empirical criterion (yet without a theoretical justification) for predicting the transition to macroscopic bubbling. Using again the equation for the equilibrium size of dynamic aggregates (Eq. 1), the Wallis criterion modified for gas-fluidized beds of fine powders would be (Valverde 2013)

$$\begin{aligned} u_\phi^* &\simeq \phi \frac{1}{18} \frac{\rho_p\, g\, d_p^2}{\mu} n \left(1 - \phi Bo_g^{(3-D)/(D+2)}\right)^{n-1} Bo_g^{2/(D+2)} \\ u_e^* &\simeq \left(g d_p \phi Bo_g^{(4-D)/(D+2)}\right)^{1/2} \\ u_\phi^* &< u_e^* \text{ nonbubbling regime} \\ u_\phi^* &\simeq u_e^* \text{ at bubbling onset} \end{aligned} \tag{4}$$

In this equation the effects of gas viscosity μ and granular Bond number Bo_g on the predicted onset of bubbling become apparent. Eventually, a sufficiently large value of the gas viscosity and/or small value of the particle size may be reached for which the predicted particle volume fraction at the bubbling onset tends to zero ($\phi_b \rightarrow 0$), which means that the bed would directly transit from the nonbubbling fluidlike regime to elutriation with full suppression of the bubbling regime. Using Eq. 3 in Eq. 4 it can be shown that

$$\frac{u_e^* - u_\phi^*}{u_e^*} = 1 - 0.7n \left(\frac{D_b}{d^*}\right)^{1/2} (\phi^*)^{1/2} (1-\phi^*)^{n-1} \tag{5}$$

The boundary between SFB (solid to fluidlike to bubbling) and SFE (solid to fluidlike to elutriation) behaviors, would be given by $\min(u_e^* - u_\phi^*) = 0$, which is obtained for $D_b/d^* \sim 1$. For $D_b/d^* \lesssim 1$ it would be $\min(u_e^* - u_\phi^*) \gtrsim 0$, i.e. the fluidized bed would transit from the nonbubbling fluidlike regime to elutriation. Interestingly, and in spite of their different backgrounds, the Harrison and Wallis criteria yield coincident predictions for bubbling suppression conditions. Thus, $D_b/d^* \sim 1$ can be used as a simple criterion to delineate the SFB-SFE boundary. A physical interpretation for the SFE behavior would be that local gas pockets in the fluidlike regime cannot reach a macroscopic size before elutriation of the aggregates takes place.

THE JAMMING TRANSITION

In the limit of small gas velocities the fluidlike nonbubbling regime would be limited by jamming of the dynamic aggregates. At the fluid-to-solid (jamming) transition, these aggregates jam in a weak solid-like structure characterized by a particle volume fraction ϕ_J that, using Eq. 1, can be related to the granular Bond number Bo_g (Valverde 2013)

$$\phi_J = \phi_J^* k^{D-3} \approx \phi_J^* Bo_g^{(D-3)/(D+2)} \tag{6}$$

where ϕ_J^* is the volume fraction of the jammed aggregates. Since dynamic aggregates can be considered as low cohesive effective spheres, ϕ_J^* must be close to the random loose packing of noncohesive spheres at the limit of zero gravitational stress ($\phi_J^* <\sim 0.56$) (Valverde et al. 2004). The bed will transit from the fluidlike regime to the solid-like fluidization regime (Geldart A) when $\phi \simeq \phi_J$. If Eq. 4 had a solution for $\phi = \phi_0 \gtrsim \phi_s$, where ϕ_s is the particle volume fraction of the powder in its initial settled state, it should be expected that the fluidized bed transits directly from the initial (not expanded) state to the bubbling regime as soon as gas velocity surpasses the minimum fluidization velocity (this is the typical Geldart B behavior). In the case that $\phi_0 = \phi_b < \phi_s$, the system could exhibit an expanded nonbubbling fluidized regime and expand up to reach a particle volume fraction $\phi = \phi_b$. If $\phi_b < \phi_J$, the bed might show a fluidlike regime window and a transition to bubbling at higher gas velocities (SFB behavior). The existence of a nonbubbling fluidlike regime depends however on the necessary condition $D_b/d^* \lesssim 10$. Otherwise, the local gas bubbles in the fluidlike regime reach a macroscopic size resulting in visible bubbling just above the jamming

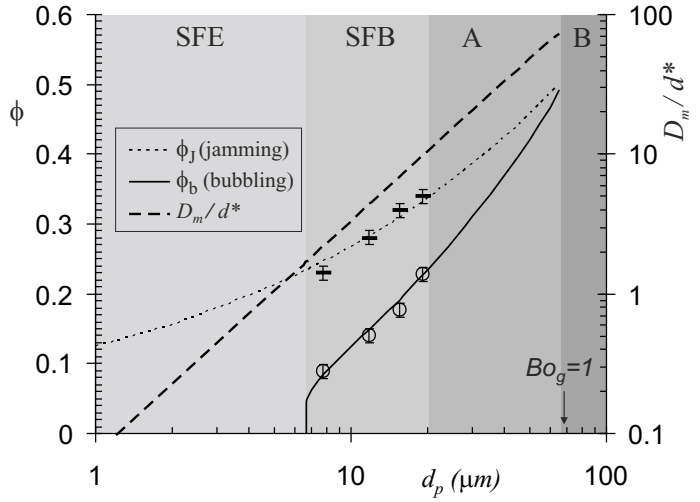

FIG. 1. Phase diagram determining the transition between the types of fluidization behavior as a function of particle size. Left axis: particle volume fraction at the jamming transition ϕ_J and at the transition to bubbling ϕ_b. Right axis: Ratio of the maximum stable size of a gas bubble to particle size. Typical values used are $\rho_p = 1135$kg/m^3, $\rho_f = 1$kg/m^3, $\mu = 1.79 \times 10^{-5}$Pa s, $F_0 = 2$nN, $g = 9.81$m/s^2, $\phi_J^* = 0.51$, and $D = 2.5$. Experimental data on the jamming and bubbling transitions for fluidized beds of conditioned xerographic toners are shown.

transition (in that case the bed would transit from the solid-like expanded fluidized state to bubbling: Geldart A behavior). Lastly, if Eq. 4 has no solution ($u_e^* > u_\phi^* \; \forall \phi > 0$ or, equivalently, $D_b/d^* \lesssim 1$), the system is expected to transit from the solid-like regime to a fluidlike regime and from the fluidlike regime to elutriation (SFE behavior). Visible bubbles would be fully suppressed in this type of fluidization.

THE MODIFIED GELDART'S DIAGRAM

In Fig. 1 the solution of Eq. 4 (particle volume fraction at the onset of bubbling ϕ_b), the solution of Eq. 6 (particle volume fraction at the jamming transition ϕ_J), and the ratio of bubble maximum size to aggregate size (D_b/d^* from Eq. 3) have been plotted vs. particle size d_p. The (typical) values used for the physical parameters intervening are $\rho_p = 1135$kg/m^3, $\mu = 1.79 \times 10^{-5}$ Pa s, $F_0 = 2$ nN, $\phi_J^* = 0.51$ and $D = 2.5$ (Valverde 2013). These values correspond to fluidization of xerographic toners of varying particle size in the range 7.8 μm $\lesssim d_p \lesssim$ 19.1 μm, using dry nitrogen at ambient conditions. Data of ϕ_J and ϕ_b from experiments on the jamming (Valverde et al. 2004) and bubbling (Valverde et al. 2003a) transitions for these powders have also been plotted. As can be seen, there is good agreement with the calculated values of ϕ_J and ϕ_b. From Fig. 1 Geldart B behavior would be predicted for $d_p \gtrsim 70\mu$m (the bed cannot expand before the onset of bubbling to a value of ϕ_J smaller than ϕ_b), Geldart A behavior for $20\mu\text{m} \lesssim d_p \lesssim 70\mu$m (in this range $\phi_J < \phi_b$, the bed expands without bubbling up to ϕ_J but large bubbles are developed in the fluidlike

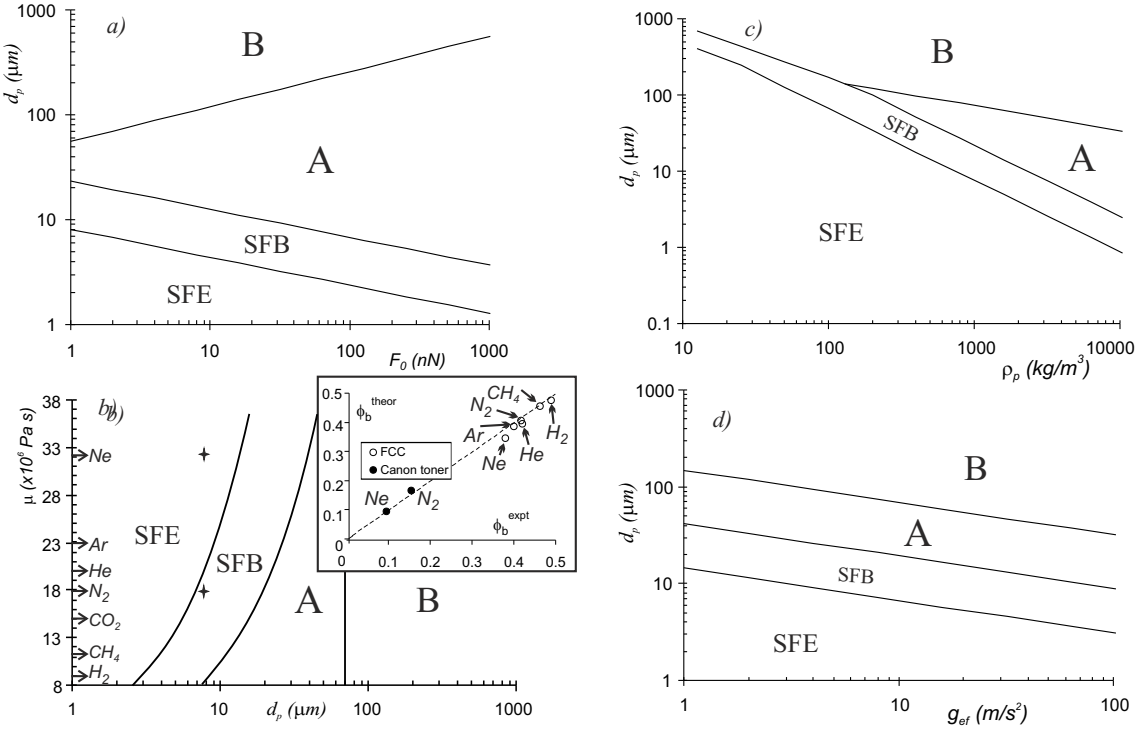

FIG. 2. Effect of interparticle force (a), gas viscosity (b), particle density (c) and effective acceleration (d) on the transition between the types of fluidization behavior as a function of particle size. Viscosity of several gases at ambient pressure and temperature are indicated in the vertical axis of (b). The symbols indicate the predicted behavior for a 7.8μm particle sized xerographic toner ($\rho_p \simeq 1135$kg/m^3, $F_0 \simeq 2$nN), showing that the SFB behavior, for fluidization with nitrogen, would shift to SFE behavior for fluidization with neon as reported experimentally. The inset of (b) shows the particle volume fraction predicted vs. experimentally measured for FCC and a Canon CLC700 toner ($\rho_p \simeq 1200$kg/m^3, $d_p = 8.6\mu$m) fluidized with different gases (indicated) at ambient conditions.

regime since $D_b/d^* \gtrsim 10$), SFB behavior for $6.7\mu\text{m} \lesssim d_p \lesssim 20\mu$m as observed for the powders tested (the bed can expand in a nonbubbling fluidlike regime since $D_b/d^* \lesssim 10$ but bubbles are developed when a particle volume fraction ϕ_b is reached), and SFE behavior for $d_p \lesssim 6.7\mu$m (there is a full suppression of the bubbling regime, $\phi_b \to 0$ and $D_b/d^* \lesssim 1$). Remarkably, the predicted A-B boundary coincides with the limit $Bo_g \simeq 1$, which according to Eq. 1 is also the limiting condition for aggregation in the fluidized bed. The criterion $Bo_g \simeq 1$ for the A-B boundary was already inferred by Molerus (Molerus 1982) from his analysis of experimental data, and by Rhodes et al. (Rhodes et al. 2001) using Discrete Element Modeling.

The effect of interparticle attractive force, gas viscosity, particle density, and effective acceleration on the types of fluidization behavior boundaries is shown in Fig. 2 (using the same typical values of the rest of parameters as in Fig. 1). Figure 2a

shows the modification in the boundaries between fluidization types as the interparticle force F_0 is increased while the rest of parameters are held constant. In agreement with experimental results, we may predict that enhancing F_0 by means of an external field can shift the behavior from Geldart B to A. For example, the interparticle attractive force between Geldart B magnetizable spheres can be increased up by application of a magnetic field, which would change their Geldart B behavior to Geldart A as seen experimentally (Espin et al. 2011). Likewise, the presence of capillary forces due to humidification of the fluidizing gas can contribute to an increase of F_0 up to $F_0 \sim 10^3$nN in a fluidized bed of fine particles (Schubert 1984), which, according to the diagram, would shift the behavior from fluidlike to Geldart A behavior as seen in experiments (Seville and Clift 1984). Interparticle attractive forces may be also increased artificially by using highly adsorbing gases (Xie and Geldart 1995), which stabilizes the (Geldart B) bubbling bed, turning its behavior into stable solidlike (Geldart A). Figure 2b shows that the SFB-SFE boundary shifts to larger particle sizes as the gas viscosity is increased. As seen experimentally, a 7.8 μm particle size xerographic toner would exhibit a transition form SFB to SFE behavior when it is fluidized by using neon instead of nitrogen (Valverde 2013). A transition to bubbling is observed for a toner with a slightly larger particle size and larger particle density (Canon CLC700 with $\rho_p = 1200$ kg/m^3 and d_p =8.6 μm). In the case of fresh cracking catalyst (FCC), with particle size around 50 μm, the observed behavior is Geldart A (Rietema 1991) as predicted. In Fig2c it is seen that the Geldart A behavior is restricted to moderate to high density particles. In the case of metallic high density beads, the Geldart B bubbling behavior is usually observed when fluidizing with a gas. For light particles the fluidization behavior would be fluidlike, either nonbubbling or bubbling. This result agrees with Harrison et al. observations, who reported nonbubbling fluidlike behavior for fluidization of phenolic micro-balloons ($\rho_p \simeq 240$kg/m^3, $d_p \simeq 125\mu$m) with CO_2 at high pressure ($\rho_f = 107$kg/m^3, μ=1.66$\times 10^{-5}$Pa s) in the interval $0.3 < \phi < 0.6$ (we predict onset of bubbling at $\phi \simeq 0.32$), and bubbling behavior with CO_2 at ambient pressure ($\rho_f = 1.6$kg/m^3, μ=1.48$\times 10^{-5}$Pa s) in the same interval (we predict onset of bubbling at $\phi \simeq 0.44$) (Harrison et al. 1961). Finally, Fig. 2d leads us to predict that the nonbubbling fluidlike behavior could be promoted in environments with reduced gravity.

The modified Geldart's diagram can be also useful to predict which type of fluidization is to be expected for fluidizable nanopowders. Recent works show that gas-fluidized beds of nanoparticles may exhibit a state of smooth, nonbubbling fluidization with high bed expansion, so-called Aggregate Particulate Fluidization (APF) state (Valverde 2013). In contrast, some nanopowders are observed to transit to a so-called aggregate bubbling fluidization (ABF) state (Valverde 2013). For example, when silica nanoparticles ($d_p = 12$ nm, $\rho_p = 2560$ kg/m^3) are fluidized with nitrogen, APF behavior is seen, whereas ABF behavior is observed for fluidization of titania nanoparticles ($d_p = 21$ nm, $\rho_p = 4500$ kg/m^3) (Zhu et al. 2005). According to the nomenclature used in this paper, the former state can be identified with the SFE (solid-to fluidlike-to elutriation behavior) type of fluidization, while the later one is identified with the SFB (solid to fluidlike to bubbling behavior) fluidization type. Empirical observations

on nonbubbling fluidlike beds of silica nanoparticles have revealed the existence of complex-aggregates formed by a multi-stage process consisting of aggregation of pre-existing simple-aggregates (Yao et al. 2002). A nanopowder typically showing this behavior is Aerosil©R974 (Evonik), which is an amorphous hydrophobic fumed silica. During flame synthesis, and due to long pathways of primary nanoparticles in the flame reactor at high temperatures, primary nanoparticles are seen to form fractal aggregates wherein they are permanently held together by strong chemical bonds because of material sintering (Hyeon-Lee et al. 1998). These aggregates have sizes on the order of microns. Subsequently, they aggregate further due to attractive van der Waals forces forming the so-called simple-aggregates of size of the order of tens of microns. In the fluidized bed, and due to van der Waals forces of attraction between them, simple-aggregates further aggregate to form complex-aggregates of size of the order of tens to hundreds of microns and density of the order of tens of kg/m^3 (Valverde and Castellanos 2008; Quintanilla et al. 2012a). Due to the small density of these complex-aggregates the nanopowder flows easily and can be fluidized by a gas in a bubble-less uniform state (Valverde and Castellanos 2007). The aggregation process of simple-aggregates into complex-aggregates may be described similarly to the dynamic aggregation of particles in conditioned fine powders by considering simple-aggregates as effective particles undergoing a dynamic process of aggregation. Thus, for nanopowder fluidization, the effective particles in fluidization are simple-aggregates (Yao et al. 2002). Typical values for the density and size of simple-aggregates for the Aerosil R974 silica nanopowder are $\rho_s \approx 50$kg/m^3 and $d_s \approx 30\mu$m (Zhu et al. 2005; Valverde and Castellanos 2006; Quintanilla et al. 2012a), which would lead us to predict SFE behavior according to the modified Geldart's diagram, in agreement with experimental observations (Valverde 2013). On the other hand, for titania nanopowder, simple-aggregates are denser (Zhu et al. 2005), which would shift the fluidization behavior to SFB as also seen experimentally (Zhu et al. 2005).

ACKNOWLEDGMENTS

This work was supported by the "Consejeria de Innovacion, Ciencia y Empresa (Junta de Andalucia)" within the European Regional Development Fund contracts FQM-5735 and by the Spanish Government Agency "Ministerio de Ciencia e Innovacion" (contract FIS2011-25161).

NOTATION

Bo_g granular Bond number

d_p particle size

d^* aggregate size

D fractal dimension

D_b largest stable size of an isolated bubble

F_0 interparticle attractive force

g gravitational acceleration

g_{ef} effective acceleration

k ratio of aggregate size to particle size

K spring constant

m_p particle mass

n Richardson-Zaki exponent

N number of particles in an aggregate

p particle-phase pressure

R_c aggregate radius

u_e elastic wave velocity

u_ϕ propagation velocity of a voidage disturbance

U_b isolated bubble rising velocity

v_{p0} settling velocity of an individual particle

v^* terminal settling velocity of an individual aggregate

W_p particle weight

GREEK SYMBOLS

β elasticity exponent

ϕ particle volume fraction

ϕ_b particle volume fraction at the onset of bubbling

ϕ_J particle volume fraction at the jamming transition

γ shear strain

μ fluid viscosity

ρ powder bulk density

ρ_f fluid density

ρ_p particle density

ρ^* aggregate density

ϕ^* volume fraction of aggregates in a fluidized bed

REFERENCES

Brooks, E. F. and Fitzgerald, T. J. (1986). *Fluidization*. Engineering Foundation, New York, Chapter Fluidization of novel tendrillar carbonaceous materials, 217 – 224.

Castellanos, A. (2005). "The relationship between attractive interparticle forces and bulk behaviour in dry and uncharged fine powders." *Adv. Phys.*, 54, 263 – 376.

Chaouki, J., Chavarie, C., Klvana, D., and Pajonk, G. (1985). "Effect of interparticle forces on the hydrodynamic behavior of fluidized aerogels." *Powder Technol.*, 43, 117 – 125.

Duru, P. and Guazzelli, E. (2002). "Experimental investigation of the secondary instability of liquid-fluidized beds and the formation of bubbles." *J. Fluid Mech.*, 470, 359 – 382.

Espin, M. J., Valverde, J. M., Quintanilla, M. A. S., and Castellanos, A. (2011). "Stabilization of gas-fluidized beds of magnetic powders by a cross - flow magnetic field." *J. Fluid Mech.*, 680, 80 113.

Foscolo, P. U. and Gibilaro, L. G. (1984). "A fully predictive criterion for the transition between particulate and aggregate fluidization." *Chem. Eng. Sci.*, 39, 1667 – 1675.

Foscolo, P. U. and Gibilaro, L. G. (1987). "Fluid dynamic stability of fluidised suspensions: the particle bed model." *Chem. Engng. Sci.*, 42(6), 1489 – 1500.

Geldart, D. (1973). "Types of gas fluidization." *Powder Technol.*, 7(5), 285–292.

Harrison, D., Davidson, J., and de Kock, J. (1961). "On the nature of aggregative and particulate fluidisation." *Trans. Inst. Chem Eng.*, 39, 202 – 211.

Hyeon-Lee, J., Beaucage, G., Pratsinis, S. E., and Vemury, S. (1998). "Fractal analysis of flame-synthesized nanostructured silica and titania powders using small-angle x-ray scattering." *Langmuir*, 14, 5751–5756.

Jackson, R. (2000). *The dynamics of fluidized particles*. Cambridge: Cambridge University Press.

Kantor, Y. and Webman, I. (1984). "Elastic properties of random percolating systems." *Phys. Rev. Lett.*, 52, 1891 – 1894.

Kantor, Y. and Witten, T. A. (1984). "Mechanical stability of tenuous objects." *J. Phys. Lett.*, 45, L675 – L679.

Koch, D. L. and Sangani, A. S. (1999). "Particle pressure and marginal stability limits for a homogeneous monodisperse gas-fluidized bed: kinetic theory and numerical simulations." *J. Fluid Mech.*, 400, 229–263.

Lepek, D., Valverde, J. M., Pfeffer, R., and Dave, R. N. (2010). "Enhanced nanofluidization by alternating electric fields." *AIChE J.*, 56, 54 – 65.

Manley, S., Cipelletti, L., Trappe, V., Bailey, A. E., Christianson, R. J., Gasser, U., Prasad, V., Segre, P. N., Doherty, M. P., Sankaran, S., Jankovsky, A. L., Shiley, B., Bowen, J., Eggers, J., Kurta, C., Lorik, T., and Weitz, D. A. (2004). "Limits to gelation in colloidal aggregation." *Phys. Rev. Lett.*, 93, 108302(1) – 108302(3).

Molerus, O. (1982). "Interpretation of geldart's type a, b, c, and d powders by taking into account interparticle cohesion forces." *Powder Tech.*, 33, 81 – 87.

Morooka, S., Kusakabe, K., Kobata, A., and Kato, Y. (1988). "Fluidization state of ultrafine powders." *J. Chem. Eng. Jpn.*, 21, 41 – 46.

Pacek, A. W. and Nienow, A. W. (1990). "Fluidisation of fine and very dense hardmetal powders." *Powder Technol.*, 60, 145 – 158.

Pfeffer, C. N. R., Dave, R. N., and Sundaresan, S. (2004). "Aerated vibrofluidization of silica nanoparticles." *AIChE J.*, 50, 1776 – 1785.

Quevedo, J., Omosebi, A., and Pfeffer, R. (2010). "Fluidization enhancement of agglomerates of metal oxide nanopowders by microjets." *AIChE J*, 56(6), 1456 1468.

Quevedo, J. A., Flesch, J., Pfeffer, R., and Dave, R. (2007). "Evaluation of assisting methods on fluidization of hydrophilic nanoagglomerates by monitoring moisture in the gas phase." *Chem. Eng. Sci.*, 62, 2608 – 2622.

Quintanilla, M. A. S., Castellanos, A., and Valverde, J. M. (2001). "Correlation between bulk stresses and interparticle contact forces in fine powders." *Phys. Rev. E*, 64, 031301(1) – 031301(9).

Quintanilla, M. A. S., Valverde, J. M., Castellanos, A., Lepek, D., Pfeffer, R., and Dave, R. (2008). "Nanofluidization as affected by vibration and electrostatic fields." *Chemical Engineering Science*, 63, 5559 – 5569.

Quintanilla, M. A. S., Valverde, J. M., and Espin, M. J. (2012a). "Electrofluidization of silica nanoparticle agglomerates." *Ind. Eng. Chem. Res.*, 51(1), 531–538.

Quintanilla, M. A. S., Valverde, J. M., Espin, M. J., and Castellanos, A. (2012b). "Electrofluidization of silica nanoparticle agglomerates." *Ind. Eng. Chem. Res.*, 51, 531 – 538.

Rhodes, M. J., Wang, X. S., Nguyen, M., Stewart, P., and Liffman, K. (2001). "Use of discrete element method simulation in studying fluidization characteristics: Influence of interparticle force." *Chem. Engng. Sci.*, 56, 69 – 76.

Rietema, K. (1991). *The Dynamics of Fine Powders*. London: Elsevier.

Schubert, H. (1984). "Capillary forces - modeling and application in particulate tech-

nology." *Powder Technol.*, 37(1), 105 – 116.

Seville, J. P. K. and Clift, R. C. (1984). "The effect of thin liquid layers on fluidization characteristics." *Powder Technol.*, 37, 117 – 129.

Sundaresan, S. (2003). "Instabilities in fluidized bed." *Annu. Rev. Fluid Mech.*, 35, 63 – 88.

Sutherland, D. N. and Tan, C. T. (1970). "Sedimentation of a porous sphere." *Chem. Eng. Sci.*, 25(12), 1948–1950.

Valverde, J. and Castellanos, A. (2008). "Fluidization of nanoparticles: A simple equation for estimating the size of agglomerates." *Chem. Eng. J.*, 140(1–3), 296–304.

Valverde, J. M. (2013). *Fluidization of Fine Powders: Cohesive versus Dynamical Aggregation*, Vol. 18 of *Particle Technology Series*. Springer.

Valverde, J. M. and Castellanos, A. (2006). "Fluidization of nanoparticles: A modified richardson–zaki law." *AIChE J.*, 52, 838 – 842.

Valverde, J. M. and Castellanos, A. (2007). "Fluidization, bubbling and jamming of nanoparticle agglomerates." *Chem. Eng. Sci.*, 62(23), 6947–6956.

Valverde, J. M., Castellanos, A., Mills, P., and Quintanilla, M. A. S. (2003a). "Effect of particle size and interparticle force on the fluidization behavior of gas-fluidized beds." *Phys. Rev. E*, 67, 051305(1) – 051305(6).

Valverde, J. M., Castellanos, A., and Quintanilla, M. A. S. (2001). "Self-diffusion in a gas-fluidized bed of fine powder." *Phys. Rev. Lett.*, 86, 3020 – 3023.

Valverde, J. M., Castellanos, A., and Quintanilla, M. A. S. (2004). "Jamming threshold of dry fine powders." *Phys. Rev. Lett.*, 92, 258303(1) – 258303(4).

Valverde, J. M., Quintanilla, M. A. S., Castellanos, A., and Mills, P. (2003b). "Experimental study on the dynamics of gas-fluidized beds." *Phys. Rev. E*, 67, 016303(1) – 016303(5).

van Ommen, J. R., Yurteri, C. U., Ellis, N., and Kelder, E. M. (2010). "Scalable gas-phase processes to create nanostructured particles." *Particuology*, 8, 572 – 577.

Witten, T. A. and Sander, L. M. (1981). "Diffusion–limited aggregation, a kinetic critical phenomenon." *Phys. Rev. Lett.*, 47, 1400 – 1403.

Xie, H.-Y. and Geldart, D. (1995). "Fluidization of fcc powders in the bubble-free regime: effect types of gases and temperature." *Powder Technol.*, 82, 269 – 277.

Yao, W., Guangsheng, G., Fei, W., and Wu, J. (2002). "Fluidization and agglomerate structure of sio_2 nanoparticles." *Powder Technol.*, 124, 152 – 159.

Yu, Q., Dave, R. N., Zhu, C., Quevedo, J. A., and Pfeffer, R. (2005). "Enhanced fluidization of nanoparticles in an oscillating magnetic field." *AIChE J.*, 51, 1971 – 1979.

Zhu, C., Liu, G., Yu, Q., Pfeffer, R., Dave, R., and C., C. N. (2004). "Sound assisted fluidization of nanoparticle agglomerates." *Powder Technol.*, 141, 119 – 123.

Zhu, C., Yu, Q., Dave, R. N., and Pfeffer, R. (2005). "Gas fluidization characteristics of nanoparticle agglomerates." *AIChE J.*, 51, 426 – 439.